SIMULATION OF EARTH'S RADIATION DURING SOLAR PROTON EVENTS IN THE PROCESS OF GEOMAGNETIC REVERSAL

© 2025 N.N. Levashov [a*], O.O. Tsareva [a], V.Yu. Popov [a,b,c], H.V. Malova [a,d], L.M. Zelenyi [a]

[a]*Space Research Institute, Moscow, Russia*

[b]*Lomonosov Moscow State University, Physical Faculty, Moscow, Russia*

[c]*HSE University, Moscow, Russia*

[d]*Scobeltsyn Institute of Nuclear Physics of Lomonosov MSU, Moscow, Russia*

**e-mail: nn.levashov@physics.msu.ru*

Received November 06, 2023
Revised May 06, 2024
Accepted June 07, 2024

Abstract. The radiation from galactic and solar cosmic rays as they pass through the modern and rarefied (as a result of multiple reversals) atmosphere during solar proton events and at the time of geomagnetic reversal is studied. We assume that during the reversal process the geomagnetic field weakens and takes on an axisymmetric quadrupole configuration. It is shown that in the case of a single reversal, when the atmosphere does not have time to change, radiation dose powers increase only at low latitudes and are identical to the modern radiation at the poles. However, during the period of multiple inversions, when the atmosphere is rarefied, the level of radiation at the moment of reversal on the Earth's surface increases, on average, twice as much as today's radiation at all latitudes, which can affect the biosphere

Keywords: *geomagnetic reversal, atmosphere, radiation*

DOI: 10.31857/S00234206250107e2

INTRODUCTION

Cosmic rays (CR) are flows of high-energy charged particles, mainly protons, creating natural cosmic radiation. CR charged particles actively bombard Earth, invading its atmosphere, and transfer their energy to matter either through ionization or through cascade formation via inelastic collisions with air nuclei [1]. CR can be divided into galactic (GCR) and solar (SCR). GCR are charged particles accelerated in our Galaxy. The energy of GCR protons (according to various theoretical estimates) ranges from 10 MeV to 10^{15}-10^{17} eV. Charged particles with even higher energy are accelerated outside our Galaxy and are called extra-galactic. SCR are charged particles accelerated in solar flares and in the shock waves they cause. SCR energy extends from fractions of MeV to (very rarely) several tens of GeV. SCR intensity is not constant and depends on solar activity: any increases in SCR intensity, both small and powerful, are called solar proton events (SPE) [2, 3]. For powerful SPEs, the energy ($E_{SCR/GCR}$) at which SCR intensity exceeds GCR intensity can reach about 100 MeV. If SPEs are powerful and their $E_{SCR/GCR}$ is very high (as, for example, in December 2006), such events are observed on Earth's surface and have a separate name - Ground Level Events (GLE). g.), such

events are observed on the surface of the Earth and there is a separate name for them - Ground Level Events (GLE).

The geomagnetic field and dense atmosphere protect our planet from CR by deflecting and absorbing charged particles. Additionally, the magnetic field prevents atmospheric erosion by the solar wind. However, the geomagnetic field is not static and has been subject to continuous changes since its inception, the most significant of which is geomagnetic reversal, i.e., polarity change. Geomagnetic reversals occur chaotically with intervals from tens of thousands to millions of years and with durations from several hundred to hundreds of thousands of years. Long periods of quiet geomagnetic field can be followed by several short periods of reversals.

Paleontological data indicate variable atmospheric density throughout Earth's history, as well as some correlation between atmospheric and geomagnetic changes. According to a widespread concept [4], geomagnetic reversals contribute to atmospheric loss, which due to the cumulative effect over several million years of multiple inversions can lead to a significant decrease in atmospheric density [5].

In one of the previous studies by the authors of this paper, the radiation environment during inversion was considered, the atmosphere was assumed to be constant, and it was shown that even when the magnetic shield weakens, the atmosphere continues to effectively absorb cosmic rays [6]. This scenario corresponded to a single inversion expected in the future.

The purpose of this study is to estimate the radiation doses of GCR and SCR when passing through the modern and rarefied (as a result of multiple inversions) atmosphere during solar proton events and at the time of geomagnetic inversion, and to compare with the current radiation environment.

NUMERICAL MODEL

To simulate primary GCR particles, the GOST 25645.150-90 standard was used. In the model of this work, it was assumed that GCR consists of 92% protons and 8% helium nuclei. The event that occurred on December 13, 2006, i.e. almost at the minimum of solar activity, was analyzed as an SPE. The spectrum of this event can be modeled using the Weibull function $W(E) = kE^{b-1}\exp\left\{-\left(E/E_0\right)^b\right\}$ [m $^{-2}$ sr $^{-1}$ s $^{-1}$ MeV $^{-1}$], where the coefficient $k = 2\cdot10^{7}$; exponent $b = 0.26$; spectrum break energy $E_0 = 0.1$ MeV [7]. The energy spectra of primary GCR and SCR particles during SPE are presented in Fig. 1.

Fig. 1. Spectra of primary GCR protons (black solid curve), alpha particles (red curve) of GCR during solar minimum, and SCR protons during SPE (black dotted curve).

For modeling cosmic ray passage through the atmosphere, the GEANT4 toolkit was used — a package for modeling the passage of elementary particles through matter using the Monte Carlo method [8]. Particle and matter interactions were described using FTFP — a list of BERT-HP physical processes. This physical model includes the Fritiof model for particles with energies above 10 GeV, the Bertini cascade model for energies below 10 GeV, and a high-precision neutron model for energies below 20 MeV [9].

For atmospheric parameterization, the empirical model NRLMSISE-00 [10] was used, which allows setting temperatures and densities of atmospheric components from the planet's surface at different latitudes. Fig. 2 shows the dependence of temperature and pressure on altitude at middle latitudes.

Fig. 2. Dependence of temperature (black dotted curve) and pressure (red solid curve) of the modern atmosphere on altitude

To determine the cosmic ray spectrum at the Earth's atmosphere boundary, Størmer theory [11, 12] was used, which showed good agreement with the results of numerical modeling of charged particle trajectory movements in the modern geomagnetic field and during its inversion [6, 13].

The dynamics of charged particles in a magnetic field is characterized by magnetic rigidity $R = pc/|q|$, where R — is the particle rigidity in GV; p — is its momentum; c — is the speed of light; $|q|$ — is the particle charge. Particles with the same rigidity have the same Larmor radius $\rho = RB = pc/|q|B$ and move along identical trajectories. The minimum rigidity at which a charged particle from space can reach a given point in near-Earth space is called the geomagnetic cutoff rigidity R_c.

The flux of charged CR particles entering from space at the Earth's atmosphere boundary is determined by the geomagnetic cutoff rigidity R_c: the lower the value of R_c, the higher the CR flux. According to Störmer's theory for a dipole magnetic field, the geomagnetic cutoff rigidity is maximum at the geomagnetic equator and decreases with increasing latitude (the so-called latitude effect) [14]. For an axisymmetric quadrupole field, the maximum geomagnetic cutoff rigidity is reached at the magnetic latitude $\lambda = \pm 26.565^{\circ}$ [12]. Vertical rigidity is a good estimate of global rigidity averaged over all directions. The values of R_c for particles vertically falling on a sphere with radius r (Earth radius r_E = 6371 km) at the geomagnetic latitude λ, equals $R_c^{dip} = cg_1^0 r_E / (4q)\,(r_E / r)^2 \cos^4 \lambda$ and $p_{quad}c = cg_2^0 r_E 1.08 / q\,(r_E / r)^3 \cos^3 \lambda \sin^{3/2} \lambda$ for dipole and quadrupole magnetic fields with Gauss coefficients g_1^0 and g_2^0 respectively [12, 13]. Figure 3 shows the cutoff energies of protons for a dipole with $g_1^0 = 30$ μT ($cg_1^0 r_E / (4e) = 14.3$ GV) and a quadrupole with $g_2^0 = 2.5$ μT ($cg_2^0 r_E 1.08 / e = 5.16$ GV) at the Earth's surface as a function of latitude λ.

Fig. 3. Geomagnetic cutoff rigidity of axisymmetric dipole and quadrupole magnetic fields versus magnetic latitude

According to the geodynamo model [15], during the inversion process, the dipole component of the field weakens by an order of magnitude, and the quadrupole component becomes dominant. Several paleomagnetic studies [16, 17] indicate a geomagnetic field with intensity less than 10% of the current intensity during the period of multiple inversions from 3.36 to 3.03 million years ago. Since the quadrupole field also evolves over time, its magnitude and configuration at the moment of inversion can, generally speaking, be random [18]. We assume an axisymmetric quadrupole configuration with a Gauss coefficient $g_2^0 = 2.5$ μT. This configuration is interesting because a tunnel-like cusp forms in the subsolar region, through which CR can effectively penetrate into the magnetosphere. In the modern era, CR fluxes on Earth decrease when moving from polar regions to the equator.

Note that besides the geomagnetic cutoff, there is also an atmospheric cutoff, for which the minimum energy of primary CR particles necessary for the formation of secondary hadronic particles reaching the Earth is ≥100 MeV [19]. Thus, the atmospheric cutoff predominates over the geomagnetic one near the magnetic poles.

Two inversion scenarios were considered: in the first scenario, the atmosphere does not change, which is characteristic of a single inversion; in the second scenario, the mass of oxygen O_2 decreases by 33%, and the mass of nitrogen N_2 by 2%, which corresponds to a 9% drop in atmospheric pressure. Such rarefaction was observed in the past during multiple inversions, likely contributing to atmospheric dissipation. During the Phanerozoic, when the frequency of inversions increased, the level of O_2 significantly decreased from the current 21% to 14% [5]. During this geological period, no noticeable variations in atmospheric N_2 were detected [20]. However, satellite data indicate that under quiet solar / geomagnetic conditions, the outflow of N^+ ions from the ionosphere is about 10% of the outflow of O^+ ions, and under disturbed conditions may even exceed it [21]. The variability of atmospheric pressure in the Phanerozoic era is also confirmed by paleontological studies [22].

SIMULATION RESULTS

The radiation carried by CRs, even today with a strong geomagnetic field, can negatively affect the operation of high-tech equipment located near the poles. In order to understand what radiation levels humanity may face during an inversion, this study calculated radiation dose rates from GCRs and SCRs during SPEs for various scenarios at key altitudes. GCRs, possessing high energy, pass the geomagnetic cutoff threshold at all latitudes even with a strong geomagnetic field. In Fig. 4. shows the radiation dose rates from GCR in μSv/hour as a function of latitude λ at an altitude of 10 km, where airplanes typically fly. The black graph shows radiation dose rates for the modern era, green - for the case of a single inversion, red - for the case of multiple inversions when the atmosphere is rarefied. The graphs show that a significant difference in radiation at this altitude for both inversion scenarios will be observed only at low latitudes.

Fig. 4. Radiation dose rates from GCR at an altitude of 10 km for protons (a), neutrons (b), muons (c) and electrons (d).

Fig. 5. shows the radiation dose rates from GCR in μSv/hour as a function of latitude at the Earth's surface for muons (a) and neutrons (b). Fig. 6 shows the total radiation dose rates from GCR in μSv/hour as a function of latitude at an altitude of 10 km and at the Earth's surface. The black graph shows dose rates for the modern era, green - for the case of a single inversion, red - for the case of multiple inversions when the atmosphere is rarefied. For the single inversion scenario, increased radiation levels will be observed only at low latitudes; however, in the case of multiple inversions, radiation levels will be several times higher compared to modern levels at all latitudes.

Fig. 5. Radiation dose rates from GCR at the Earth's surface for muons (a) and neutrons (b).

Fig. 6. Total radiation dose rates from GCR at an altitude of 10 km (a), at the Earth's surface (b).

The dashed blue graph shows radiation dose rates for the modern era calculated using the semi-empirical PARMA model [23]. The difference in dose rates for the modern era obtained in this study and calculated using PARMA is due to the fact that the model used in this study does not account for

the contribution of albedo protons to radiation, and also, in primary GCR, we neglect atomic nuclei heavier than helium. In addition, due to the specifics of the GEANT4 package, in the model of this study, the atmosphere is divided into layers. Average atmospheric parameters corresponding to the altitude of each layer are simulated within each layer. Such a discrete division of the atmosphere can also affect the final simulation result.

SCL particles have much lower energy compared to GCR. However, during strong SEP events, solar protons with energy exceeding the geomagnetic cutoff threshold at middle latitudes may prevail over GCR protons. Fig. 7 shows the dose rates for the selected SEP event depending on latitude at an altitude of 10 km for protons (a), neutrons (b), electrons (c), and total dose rates for all particles (d).

Fig. 7. Radiation dose rates from SCL during SEP event at an altitude of 10 km for protons (a), neutrons (b), electrons (c), total for all particles (d).

Fig. 8 shows the radiation dose rate depending on latitude at the planet's surface. The black graph displays the dose rate in nanosieverts for the modern epoch, green - for the case of a single inversion, red - for the case of multiple inversions when the atmosphere is rarefied. For this SEP event, only neutrons were able to reach the Earth's surface; the radiation contribution from other particles is negligibly small.

Fig. 8. SCL radiation dose rate during SEP event for neutrons at the Earth's surface.

CONCLUSION

This paper examines the change in the radiation environment in near-Earth space during geomagnetic inversion. For the case of a single inversion, when the geomagnetic field weakens briefly on a geological scale and atmospheric density does not have time to change, the radiation level increases only at latitudes close to the equator. This spatial distribution of radiation is due to the axisymmetric quadrupole configuration of the magnetic field. For the case of multiple inversions, when the geomagnetic field is weakened long enough for the solar wind to disperse part of the atmosphere, radiation doses from GCR increase at all latitudes and are 2-3 times higher than current levels at the planet's surface. During SEP events, the radiation level at the magnetic poles (i.e., in the absence of geomagnetic cutoff) is 2-3 times higher than during periods of low solar activity.

FUNDING

This work was supported by grant MK-5053.2022.6 from the Ministry of Science and Higher Education of the Russian Federation.

REFERENCES

1. *Maurchev E.A., Balabin Yu.V., Germanenko A.V., et al.* Impact of cosmic ray protons on the formation of secondary particles and ionization in the Earth's atmosphere // Proceedings of the Kola Science Center of the Russian Academy of Sciences. 2019. Vol. 10. No. 8(5). P. 240–249. DOI: 10.25702/KSC.2307-5252.2019.10.8.240-249

2. *Snyder C.W., Neugebauer M., Rao U.R.* The solar wind velocity and its correlation with cosmic ray variations and with solar and geomagnetic activity // J. Geophys Res. 1963. V. 68. Iss. 34. P. 6361–6370. DOI: 10.1029/JZ068i024p06361

3. *Krivolutsky A.A., Repnev A.I.* Impact of cosmic energetic particles on the Earth's atmosphere (review) // Geomagnetism and Aeronomy. 2012. Vol. 52. No. 6. P. 723–754.

4. *Dehant V., Lammer H., Kulikov Y.N. et al.* Planetary Magnetic Dynamo Effect on Atmospheric Protection of Early Earth and Mars // Space Science Reviews. 2007. V. 129(1-3). P. 279–300. DOI: 10.1007/s11214-007-9163-9

5. *Wei Y., Pu Z., Zong Q.-W. et al* . Oxygen escape from the Earth during geomagnetic reversals: Implications to mass extinction // Earth and Planetary Science Letters. 2014. V. 394. P. 94–98. DOI: 10.1016/j.epsl.2014.03.018

6. *Tsareva O.O., Zelenyi L.M., Malova Kh.V. et al* . What awaits humanity during the Earth's magnetic field inversion: imaginary and genuine threats // Physics-Uspekhi. 2018. No. 188. P. 207–220. DOI: 10.3367/UFNr.2017.07.038190

7. *Laurenza M., Consolini G., Storini M. et al* . The Weibull functional form for SEP event spectra // J. Physics Conference Series. 2015. V. 632. Art.ID 012066. DOI:10.1088/1742-6596/632/1/012066

8. *Agostinelli S., Allisonas J., Amako K. et al.* Geant4 - A Simulation Toolkit // Nuclear Instruments and Methods in Physics Research . 2003. V. 506. P. 250–303. DOI:10.1016/S0168-9002(03)01368-8.

9. *Allison J., Amako K., Apostolakis J. et al* . Recent developments in geant4 // Nuclear Instruments and Methods in Physics Research. Section A. 2016. V. 835. P. 186–225. https://doi.org/10.1016/j.nima.2016.06.125, DOI:10.1016/j.nima.2016.06.125.

10. *Picone J., Hedin A.E., Drob D. et al.* NRLMSISE-00 empirical model of the atmosphere: Statistical comparison and scientific issues // J. Geophysical Research. 2002. V. 107. Iss. A12. Art.ID. 1468. DOI:10.1029/2002JA009430

11. *Störmer C* . The polar Aurora. Oxford: Clarendon Press, 1955.

12. *Tsareva O.O.* Generalization of Störmer theory for an axisymmetric superposition of dipole and quadrupole fields // J. Geophysical Research: Space Physics. 2019. V. 124. P. 2844–2853. DOI:10.1029/2018JA026164

13. *Stadelmann A., Vogt J., Glassmeier K.H. et al* . Cosmic ray and solar energetic particle flux in paleomagnetospheres // Earth Planets and Space. 2010. V. 62. P. 333–345. DOI:10.5047/eps.2009.10.002

14. *Murzin V.* Astrophysics of cosmic rays. Moscow: University Book; Logos, 2007.

15. *Glatzmaier G.A., Roberts P.H.* A three-dimensional convective dynamo solution with rotating and finitely conducting inner core and mantle // Physics of the Earth and Planetary Interiors . 1995. V. 91. Iss. 1. P. 63 – 75. DOI: 10.1016/0031-9201(95)03049-3

16. *Valet J.-P., Thevarasan A., Bassinot F. et al.* Two records of relative paleointensity for the past 4 Myr. // Frontiers in Earth Science. 2020. V. 8. Iss. 148. DOI: 10.3389/feart.2020.00148

17. *Herrero-Bervera E., Valet J.-P.* Absolute paleointensity and reversal records from the Waianae sequence (Oahu, Hawaii, USA) // Earth and Planetary Science Letters. 2005. V. 234. Iss. 1–2. P. 279–296. DOI:10.1016/j.epsl.2005.02.032

18. *Poluianov S., Batalla O.* Cosmic-ray atmospheric cutoff energies of polar neutron monitors // Advances in Space Research. 2022. V. 70. Iss. 9. P. 2610–2617. DOI: 10.1016/j.asr.2022.03.037

19. *Vogt J., Glassmeier K. H* . On the location of trapped particle populations in quadrupole magnetospheres // J. Geophysical Research: Space Physics. 2000. V. 105. Iss. A6. P. 13063–13071. DOI:10.1029/2000ja900006

20. *Berner R. A.* Geological nitrogen cycle and atmospheric N2 over Phanerozoic time // Geology. 2006. V. 34. Iss. 5. Art.ID. 413. DOI:10.1130/g22470.1

21. *Ilie R., Liemohn M.W.* The outflow of ionospheric nitrogen ions: A possible tracer for the altitude dependent transport and energization processes of ionospheric plasma // J. Geophysical Research: Space Physics. 2016. V. 121. P. 9250–9255. DOI:10.1002/2015JA022162

22. *Cannell A., Nel A.* Paleo-air pressures and respiration of giant Odonatoptera from the Late Carboniferous to the Early Cretaceous // Palaeoentomology. 2023. V. 6. Iss. 4. DOI: 10.11646/palaeoentomology.6.4.6

23. *Sato T., Yasuda H., Niita K. et al.* Development of PARMA: PHITS-based analytical radiation model in the atmosphere // Radiation research. 2008. V. 170. Iss. 2. P. 244–259. DOI: 10.1667/RR1094.1.

FIGURE CAPTIONS:

Fig. 1. Spectra of primary GCR protons (black solid curve), GCR alpha particles (red curve) during solar minimum and SCR protons during SPE (black dashed curve).

Fig. 2. Dependence of temperature (black dashed curve) and pressure (red solid curve) of the modern atmosphere on altitude

Fig. 3. Geomagnetic cutoff rigidity of axisymmetric dipole and quadrupole magnetic fields versus magnetic latitude

Fig. 4. Radiation dose rates from GCR at an altitude of 10 km for protons (a), neutrons (b), muons (c) and electrons (d).

Fig. 5 Radiation dose rates from GCR at the Earth's surface for muons (a) and neutrons (b).

Fig. 6. Total radiation dose rates from GCR at an altitude of 10 km (a), at the Earth's surface (b).

Fig. 7. Radiation dose rates from SCR during SPE at an altitude of 10 km for protons (a), neutrons (b), electrons (c), total for all particles (d).

Fig. 8. SCR radiation dose rates during SPE for neutrons at the Earth's surface.

Figures:

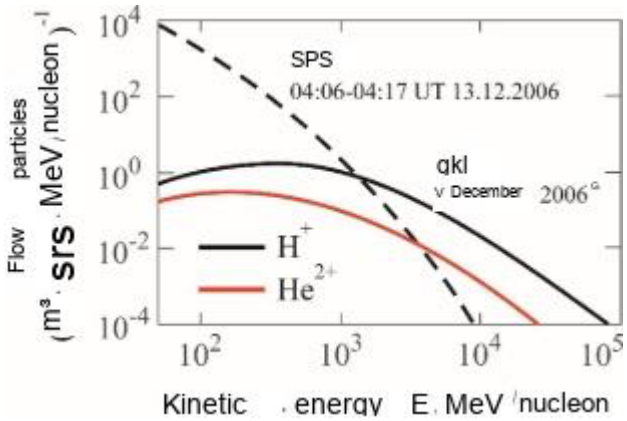

Fig.1

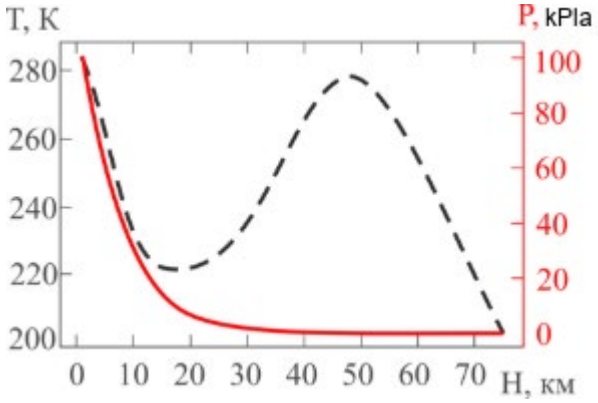

Fig.2

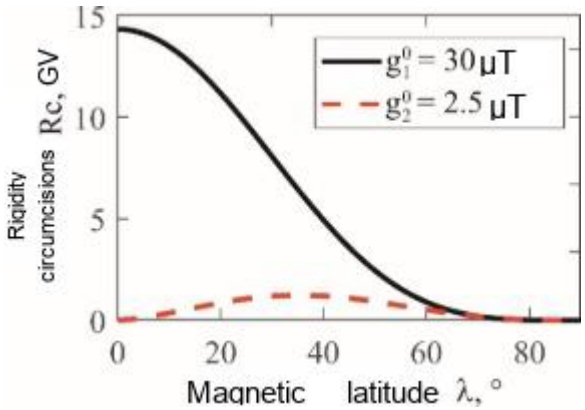
15
10
5
0
Rigidity circumcisions Rc, GV
$g_1^0 = 30\,\mu T$
$g_2^0 = 2.5\,\mu T$
0
20
40
60
80
Magnetic latitude λ, °

Fig.3

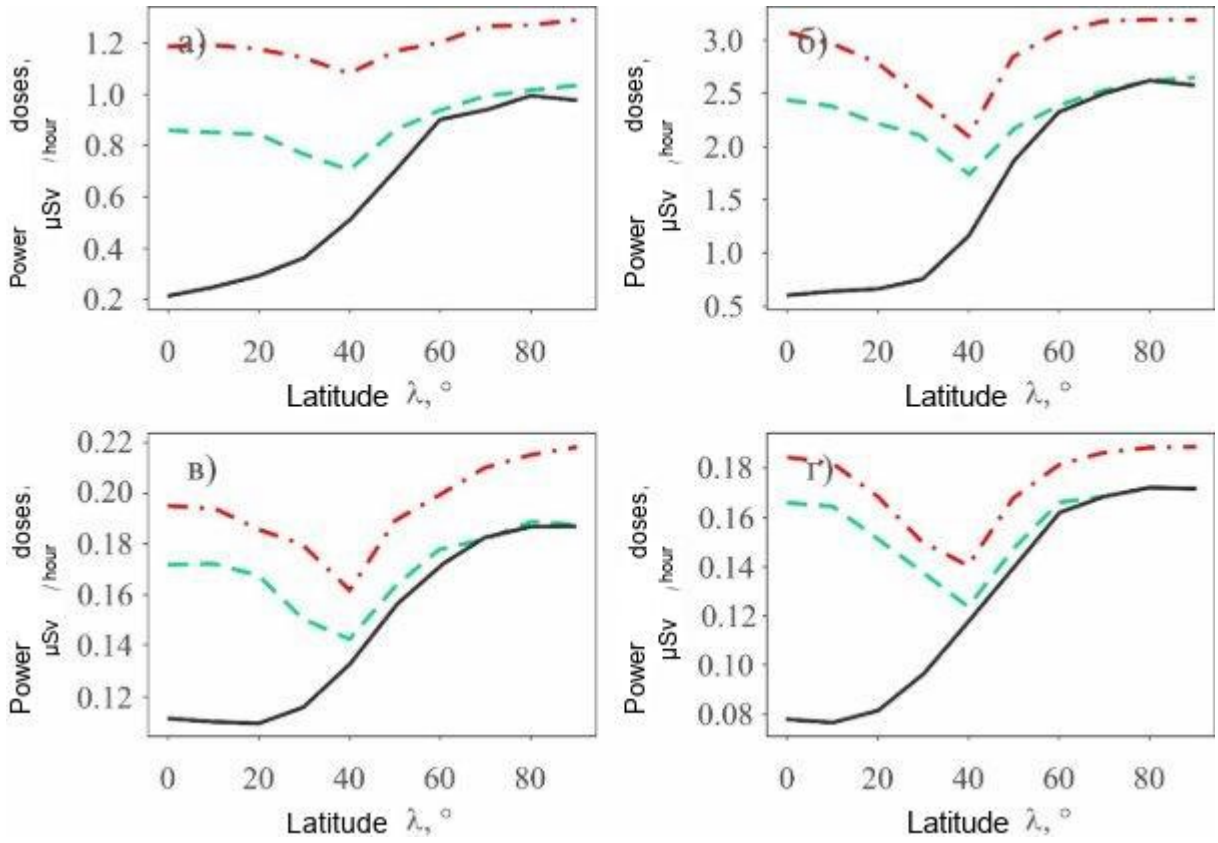
а)
б)
в)
г)
Power doses, μSv / hour
Latitude λ, °
0
20
40
60
80

Fig.4

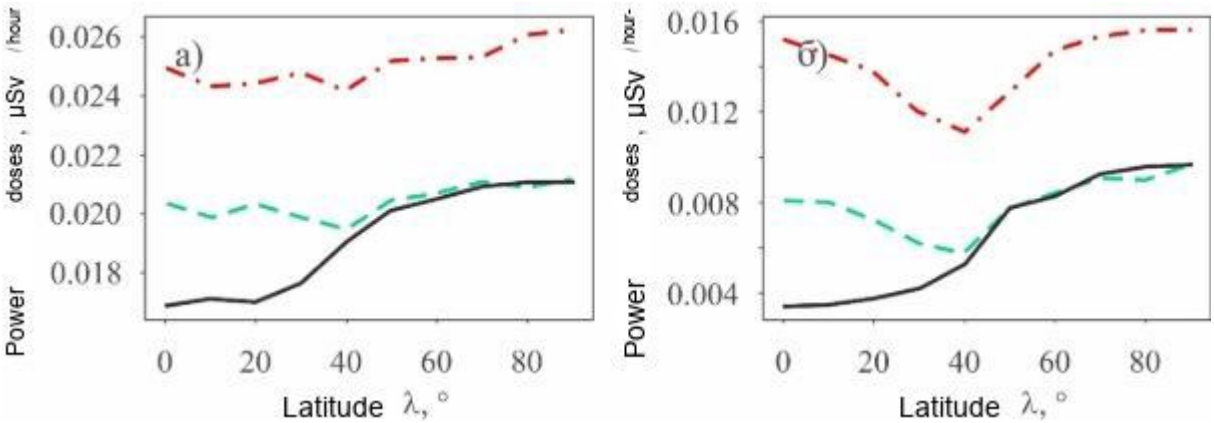
a)
0.026
0.024
0.022
0.020
0.018
Power doses, μSv/hour
0
20
40
60
80
Latitude λ, °
б)
0.016
0.012
0.008
0.004
Power doses, μSv/hour
0
20
40
60
80
Latitude λ, °

Fig.5

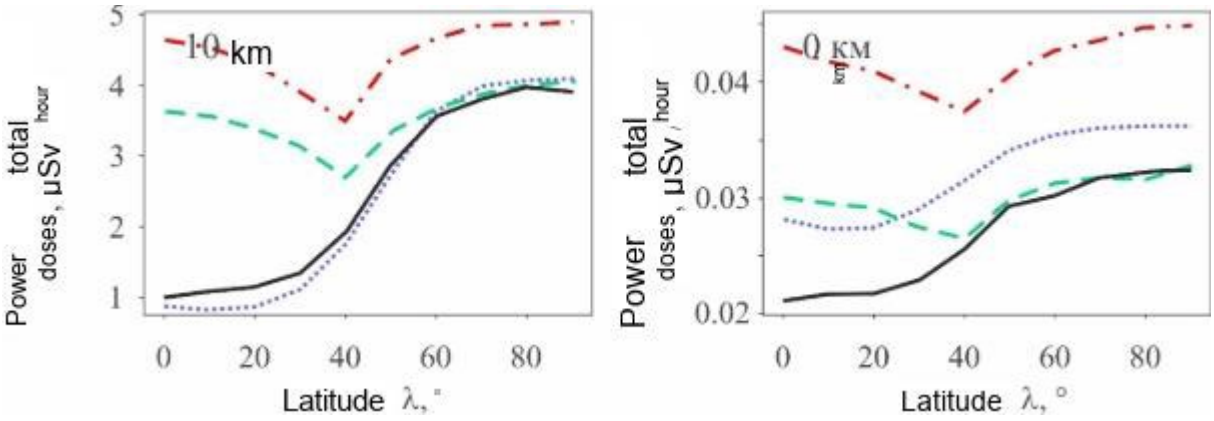
10 km
5
4
3
2
1
Power total doses, μSv/hour
0
20
40
60
80
Latitude λ, °
0 км
0.04
0.03
0.02
Power total doses, μSv/hour
0
20
40
60
80
Latitude λ, °

Fig.6

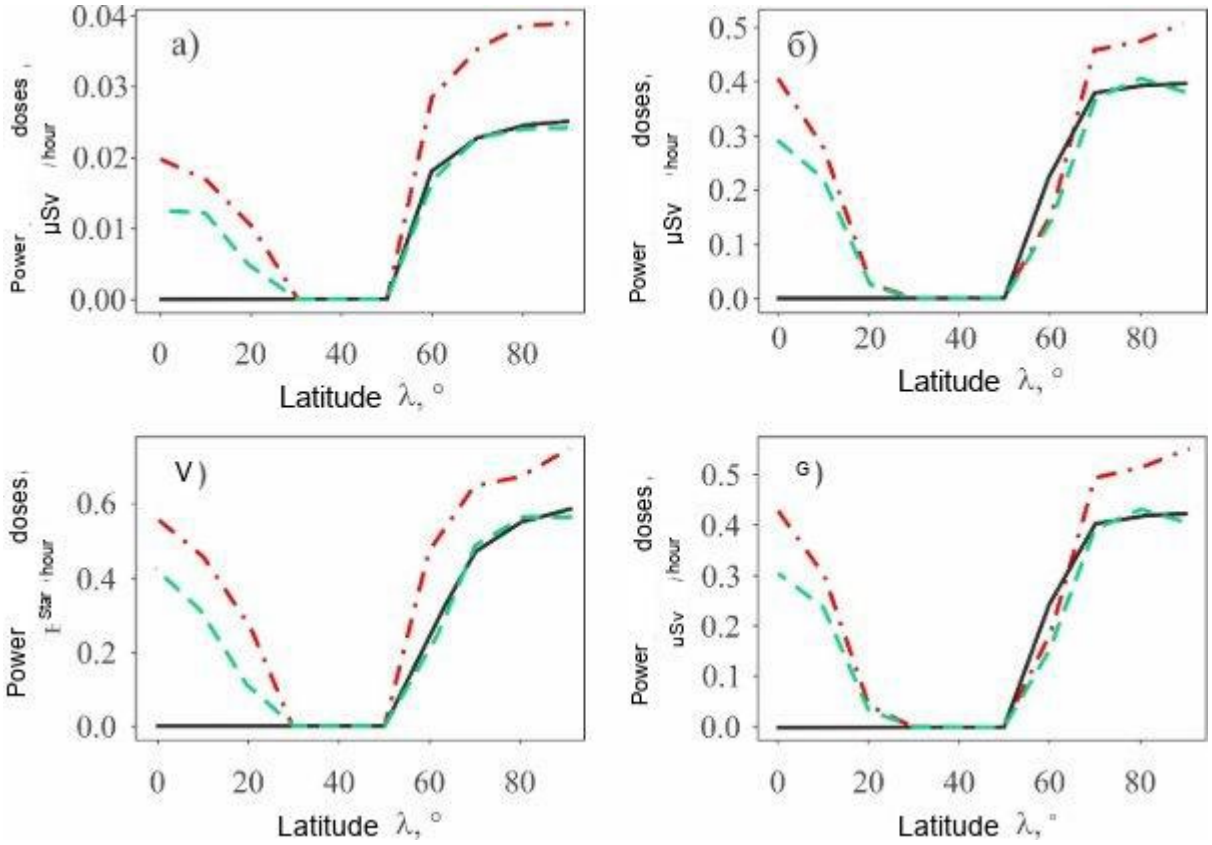
а)
б)
в)
г)
Power doses, μSv / hour
Power doses, μSv / hour
Power doses, H^{Star}, hour
Power doses, uSv / hour
Latitude λ, °
Latitude λ, °
Latitude λ, °
Latitude λ, °

Fig.7

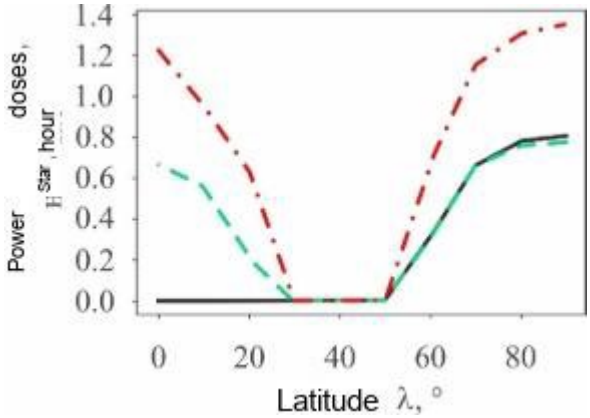
Power doses, H^{Star}, hour
Latitude λ, °

Fig.8